# Effect of crystallographic orientation on phase transformations during indentation of silicon

Y.B Gerbig[a)]
*Ceramics Division, National Institute of Standards and Technology, Gaithersburg, Maryland 20899*

S.J. Stranick
*Surface and Microanalysis Science Division, National Institute of Standards and Technology, Gaithersburg, Maryland 20899*

D.J. Morris, M.D. Vaudin, and R.F. Cook
*Ceramics Division, National Institute of Standards and Technology, Gaithersburg, Maryland 20899*

(Received 6 August 2008; accepted 25 November 2008)

In a statistical nanoindentation study using a spherical probe, the effect of crystallographic orientation on the phase transformation of silicon (Si) was investigated. The occurrence and the contact pressures at which events associated with phase transformation occur, for an indentation force range from 20 to 200 mN, were analyzed and compared for the orientations Si(001), Si(110), and Si(111). It was found that plastic deformation combined with phase transformation during loading was initiated at lower forces (contact pressures) for Si(110) and Si(111) than for Si(001). Also, the contact pressure at which the phase transformation occurred during unloading was strongly influenced by the crystallographic orientation, with up to 38% greater values for Si(110) and Si(111) compared to Si(001). Mapping the residual stress field around indentations by confocal Raman microscopy revealed significant differences in the stress pattern for the three orientations.

## I. INTRODUCTION

Single crystal silicon (Si) is one of the principal materials used for solid-state electronics, microelectromechanical systems (MEMS), infrared optical, and photovoltaic technologies. In recent decades, various solid phases of Si have been observed as a result of mechanical loading of the material.[1,2] Knowledge of the nature and occurrence of these Si phases is essential, as the performance of Si-based devices depends on the Si properties, which are strongly influenced by phase transformations. For example, Si changes its electrical characteristics from semiconductor-like to metallic under mechanical loading.[3] The entire concept of ductile-regime (DR) machining, an ultraprecision machining process applied by the semiconductor industry, is based on the transformation from the brittle (Si-I) to the ductile (Si-II) phase.[4] Phase transformations have a significant impact on the tribological performance of Si.[5] The lower etching rates of high-pressure polycrystalline phases created through phase transformation are exploited in a recent new maskless patterning process.[6]

Although earlier works (reviewed in Ref. 7) indicate a dependence of the transformation pressures on the crystallographic orientation (in other words, a dependence on the loading direction), the Si(001) orientation (and hence loading along Si[001]) has been studied almost exclusively, as it is the most common orientation used in the semiconductor microelectronics industry. In strain engineering, however, tensile or compressive stresses are induced perpendicular to the [001] direction to enhance transistor performance through enhanced carrier mobility.[8] For MEMS (especially with moving parts), loading in more than one direction simultaneously or alternately may occur during operation because of complexity in design and functionality.[9,10] Nonuniaxial, nonoperational loading must often be considered as well, for example, during the impact of hailstones[11] or micrometeoroids[12] on solar panels located on earth or space craft; Si(111) is the preferentially used orientation in the photovoltaics industry. On machining Si-based structures and devices, loading of the Si surface in different directions is inevitable due to the nature of the machining process. Especially for DR machining, information about differences in the brittle-ductile transformation pressure for the various crystallographic orientations is crucial to obtain the best results regarding subsurface damage, form accuracy, and surface finish and, hence, to guarantee the functionality and reliability of the machined structure.[13,14] As a consequence, knowledge about the effect of the crystallographic orientation

[a)]Address all correspondence to this author.
e-mail: yvonne.gerbig@nist.gov
DOI: 10.1557/JMR.2009.0122

on phase transformations of Si has gained significantly in importance and needs to be addressed in experimental studies.

Indentation techniques are a well-established method for studying phase transformations.[2] In indentation tests, a shear component is introduced in addition to the hydrostatic stress, so that these techniques may provide a loading regime closer to conditions occurring in practice compared to a purely hydrostatic pressure as applied in diamond anvil cells (another well-established method in phase transformation research). Based on analyses using transmission electron microscopy (TEM) and Raman microscopy of indented regions, it is believed that the following phase transformations take place during indentation tests at ambient conditions[2]: During loading, the "primary" phase transformation from the Si-I [diamond, face-centered-cubic (fcc)] to the Si-II (β-tin, tetragonal) phase is initiated above a certain threshold of the contact pressure [hereafter called phase transformation during loading (PTL)]. This transition is accompanied by a volume decrease of 22%. When the contact pressure is released (unloading), the Si-II phase can undergo further "secondary" transformations [hereafter called phase transformation during unloading (PTU)] to

(i) polycrystalline high-pressure phases. It is assumed that initially the Si-XII (rhombohedral with 8 atoms per unit cell, R8) phase is formed leading to 9% volume expansion. On further contact pressure release, Si-XII is partially transformed to the SI-III [body-centered-cubic (bcc) with 16 atoms per unit cell, BC8] resulting in a mixture of Si-XII and Si-III.

(ii) amorphous phase, *a*-Si.

The predominance of one or the other secondary phases in the transformed region depends strongly on the test conditions applied during the indentation, e.g., maximum force, unloading rate, and indenter geometry.[2,15] However, due to the inhomogenity in stress distribution and variations in crystal defect concentration, a mixture of Si-XII + Si-III + Si-I + *a*-Si is often found in the indented region.[16] Certain phase transformations can be associated with specific discontinuities in the loading and unloading branches of the indentation test.[2]

The effect of crystallographic orientation on the phase transformations has been the subject of only a few indentation studies, with partially inconsistent results. Several groups reported similar trends regarding the various crystallographic orientations,[17,18] whereas the results of other groups gave evidence for a dependence on the crystallographic orientation.[7,19]

In this work, the effect of the crystallographic orientation on the phase transformations of Si during indentation loading and unloading is investigated in a statistical study of tests using a spherical indenter. The presence of, and the pressure at which events associated with phase transformation occur in the (un)loading segment of the indentation curve, are analyzed and compared for three orientations, Si(001), Si(110), and Si(111), in an indentation force range from 20 to 200 mN. Confocal Raman microscopy is used to map the residual stress field around indentations produced in various loading directions.

## II. EXPERIMENTAL

### A. Nanoindentation experiments

To study the effects of indentation loading direction, Czochralski grown Si(001), Si(110), and Si(111) wafers were tested (Virginia Semiconductor, Inc., Fredericksburg, VA). The wafers, diameter of 35 mm and thickness of 3 mm, were doped with phosphorous to a resistivity of 1 to 20 Ω cm and were those used in a previous indentation fracture study.[20] The indentation experiments were carried out with a conospherical diamond indenter with a nominal tip radius of 5 μm using a TI 900TriboIndenter (Hysitron, Inc., Minneapolis, MN) in a nitrogen-rich atmosphere (temperature: 21 ± 1 °C, relative humidity: 5 ± 1%). The indenter was displaced perpendicular to the Si(001), Si(110), and Si(111) planes of the wafers, which resulted in loading along the Si[001], Si[011], and Si[111] directions. In all tests, the applied force $P$ and the corresponding displacement $h$ were continuously recorded. Prior to every test, the thermal drift was determined for a time period equal to the duration of the indentation.

A conospherical indenter was used as indenters with a spherical tip produce a more uniform stress field and are less likely to cause cracking during indentation than pointed indenters. In contrast to pointed indenters that generate contact pressures great enough to initiate the primary phase transformation immediately on contact with the sample, this transformation may be observable during loading with a spherical indenter.[21,22]

To capture the effects of varying indentation loads, the various maximum forces (20, 25, 30, 45, 60, 80, 100, 150, and 200 mN) were applied in a continuous loading-unloading technique for all three crystallographic orientations. During the indentation test the force was linearly increased with time to the maximum value, held for 5 s, and linearly decreased. The loading and unloading rates were fixed at 5 mN $s^{-1}$ in all tests (data acquisition rate 50 Hz). For each maximum force, 50 indentation tests were performed. The indentations were positioned 50 μm apart.

To study the onset of the primary phase transformation, tests were carried out in the multiple partial unloading techniques, as developed by Field and Swain.[23] In this technique the force is stepwise increased, but before continuing to the next, greater, force value, the force is partially released. The resulting force–displacement curve has two branches corresponding to the fully loaded

points and the partially unloaded points. For elastic deformation, the two branches coincide, but they diverge on plastic deformation. As the plastic deformation of Si starts with a phase transformation, this technique enables the assessment of the onset of the primary phase transformation. In this study, the force was increased to 50 mN in 50 steps. In-between the loading steps, the load was released to 75% of its value. The loading and unloading were realized in 1 s every cycle (data acquisition rate 50 Hz). For every orientation, 50 tests were carried out; the tests were positioned 50 μm apart.

To calculate the event pressure (see Sec. III. B), the effective tip radius of the indenter at a given penetration depth needs to be known. Therefore, the indenter tip was scanned in two perpendicular directions on a calibrated atomic force microscope (AFM) (MFP-3D; Asylum Research, Santa Barbara, CA). The scan area and scan rate were set to 10 μm × 10 μm and 10 μm $s^{-1}$, respectively. The AFM cantilever probes were made of Si with a nominal tip curvature of 10 nm, a typical resonance frequency of 325 kHz and a typical spring constant of 40 N $m^{-1}$. Prior to imaging, the surface of the diamond indenter tip was cleaned by a carbon dioxide snow jet to remove hydrocarbons and small particles bound by adhesion.[24] Using the image processing software package SPIP (Image Metrology A/S, Hørsholm, Denmark), the tip curvature at a series of height steps from the apex was determined from the AFM images. The height ranges were defined by consideration of the penetration depths recorded in the indentation tests. By fitting several curvature-height data plots, an empirical equation between the effective indenter tip radius and penetration depth was found.

### B. Raman microscopy

The indented Si wafers were imaged by hyperspectral, confocal Raman microscopy (CRM). The CRM measurements were performed on an in-house designed system, which was based on a setup described in detail elsewhere.[25] Briefly, the samples were illuminated by laser radiation passed through a polarizer and an "inject-reject" style notch filter and focused on the sample using a 60× oil immersion lens of numerical aperture 1.4. Scattered Raman light was collected by the lens, passed back through the notch filter, and collected with a high resolution spectrograph (better than 2 $cm^{-1}$ resolution). Single-mode optical fibers coupled the laser and spectrograph to the system to provide an input Gaussian beam and confocal collection of the output scattered light. An *x-y* stage with closed-loop control with 10-nm resolution allowed for scanning of the sample; with oversampling, the spatial resolution of the technique was sub-200 nm. A Nd:YAG excitation laser with a wavelength of 532 nm was used. The sampling depth (penetration depth × escape depth) for this wavelength was 400 nm for (Si-I), but was assumed to be smaller for *a*-Si and other phases because of their greater signal absorbance.[22]

The illumination power was set to 2 mW at the sample surfaces with the polarization axis positioned along the ⟨110⟩, ⟨100⟩, or ⟨112⟩ directions for Si(001), Si(110), and Si(111), respectively (or along the vertical axes in the images presented here). The spectral acquisition time was 1.5 s, which resulted in an average signal-to-noise ratio of 2500:1. The hyperspectral images comprised 128 ×128 (16384) spectra. The individual spectra were fit using a Pearson7 function implemented in MatLab (The Mathworks, Inc., Natick, MA) to determine the position of the Si Raman phonon scattering peak, and the peak shifts were referenced against the peak position of a zero stress region (nominally 520.5 $cm^{-1}$). The results of the fit were then converted to stress using the constant −435 MPa/$cm^{-1}$ applicable to a uniaxial or biaxial stress field.[26] No image processing was performed other than exclusion of the data from within the indentation region (shown in stripe pattern in the images presented). On the basis of the location of other peaks present in the Raman spectra, the Si phases generated within the indentation region were identified.[27]

## III. ANALYSIS

In indentation tests, phase transformations are manifest as characteristic discontinuities (events) at specific forces (pressures) in indentation load–displacement curves. The following section describes the identification of typical events and determination of the contact pressures at which those events occur.

### A. Classification of events in indentation curves

#### 1. Events occurring during loading

As long as the contact pressure does not exceed the threshold for crack initiation, two characteristic loading events have been observed in indentation tests on Si with spherical indenters. Weppelmann[21] and Williams[28] reported a change in slope of the loading curve at contact pressures that allowed the association of this event with the primary phase transformation. Other groups found a plateaulike discontinuity in the loading curves, or so called "pop-in" event.[22,29–31] The pop-in event is presumably caused by plastic flow initiated in ductile Si-II when the volume of the transformed material extends beyond the constrained region beneath the indentation contact.[29]

#### 2. Events occurring during unloading

Following previous studies,[18,22,32] the indentation curves were differentiated into six classifications with regard to the shape of their unloading segments. The

classifications are elastic behavior (EL), plastic behavior (PL), elbow (E), pop-out (P), kink pop-out (K), and elbow followed by pop-out (EP) events.

In the case of elastic behavior, the indenter-induced deformation of the sample surface is purely elastic and, thus, loading and unloading curves of the indentation test coincide due to complete recovery of the deformation during unloading [Fig. 1(a)].

During elastic–plastic loading, residual plastic deformation leads to a divergence between the loading and unloading branches of the indentation curve. For a curve with plastic behavior (without exhibiting a PTU-related event), the unloading data can be described by the frequently used power law $P = \alpha(h - h_{\mathrm{p,\ max}})^m$ [Fig. 1(b)], where $h_{\mathrm{p,\ max}}$ is the residual plastic deformation after complete unloading and $\alpha$ and $m$ are empirical material and indenter parameters.[33]

Curves classified as elbow deviated from the previously mentioned power-law behavior by exhibiting a smooth and accelerated change of derivative at a certain load, as observed in Fig. 1(c). In the derivative plot (the instantaneous unloading compliance, shown as the dotted lines in Fig. 1), a gradual, over-proportional change of the unloading slope with decreasing depth characterizes the elbow event. The gradual change of slope is associated with material expansion during a slow amorphization of Si-II.[2]

In the case of a pop-out event, the derivative maintains a constant value until the indenter is pushed up (out of the surface) by the Si-II to Si-XII transformation-induced

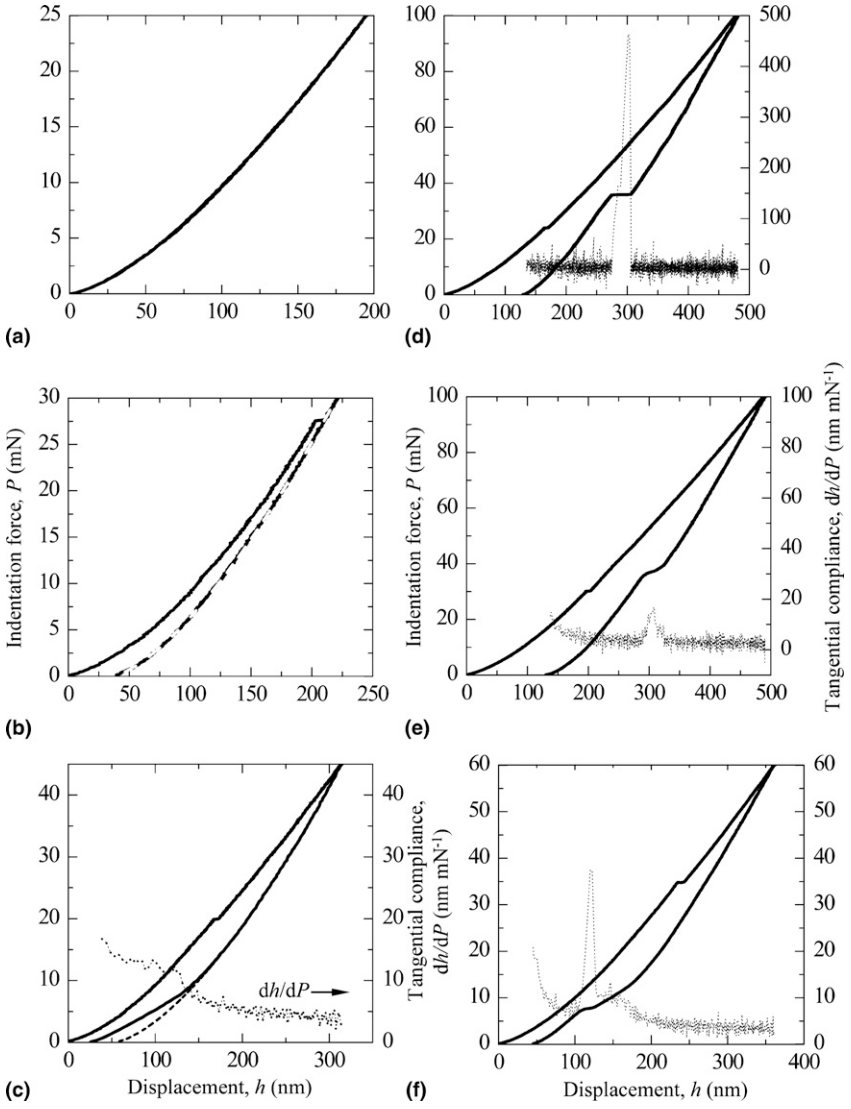


FIG. 1. Classification of characteristic shapes of the unloading segment in indentation curves: (a) elastic behavior, (b) plastic behavior, (c) elbow, (d) pop-out, (e) kink pop-out events, and (f) elbow followed by pop-out event. The graphs display the force ($P$)-displacement ($h$) curves as well as the derivative ($dh/dP$)-displacement ($h$) curves for the events (c)–(f). The fit of the upper portion of the unloading segment to the power law $P = \alpha(h–h_{\mathrm{p,max}})^m$ (see text) is shown as a dashed line in graphs (b) and (c). In graph (b), the dashed fitting line coincides with the solid line.

expansion of material underneath the indenter.[2] This event leads to the occurrence of a pronounced force plateau, while the following segment of the curve exhibits an (almost) constant derivative again [Fig. 1(d)]. In the derivative plot, the derivative suddenly increased more than one order in magnitude and returned to smaller value.

A kink pop-out event occurs during a broader unloading segment and longer time span than the pop-out event [Fig. 1(e)], which implies a more gradual transformation of the material under the indenter. As a consequence, after a segment of constant derivative, the kink pop-out event appears as a slopelike feature rather than a plateau in the unloading curve. After the kink pop-out event, the unloading curve once again returns to an (almost) constant derivative. Similar to the pop-out event, the derivative suddenly increases at the onset of the kink pop-out. However, the derivative is only on the order of 40 nm $mN^{-1}$ or less.

A curve classified as elbow followed by pop-out exhibits features of both events [compare Figs. 1(c) and 1(d) with Fig. 1(f)]. In the unloading curve, the continuous derivative change (typical for elbow) is interrupted by sudden material expansion causing the occurrence of a plateau (characteristic for pop-out). The derivative of a curve with an EP event exhibits a gradual increase followed by a steep rise to a range of about 30 to 100 nm $mN^{-1}$.

### B. Calculation of event pressure

The mean contact pressure at the spherical indenter-flat sample interface was calculated for specific events using the equation

$$p_{\mathrm{m,event}} = p_{\mathrm{event}} / \left(\pi \cdot a_{\mathrm{c,event}}{}^{2}\right) \quad , \tag{1}$$

where $a_{\mathrm{c,event}}$ is the radius of the circle of contact, $P_{\mathrm{event}}$ is the event load, and $p_{\mathrm{m,event}}$ is the mean contact pressure, at which the event, e.g., PTL or PTU, occurred.

#### 1. PTL

For Si, the onset of PTL indicates the transition from purely elastic to elastic–plastic loading. Therefore, equations describing the mechanics at an elastic contact can be applied to determine $a_{\mathrm{c,PTL}}$, the radius of the contact circle for this event[21]:

$$a_{\mathrm{c,PTL}} = \left(R_{\mathrm{eff,PTL}} h_{\mathrm{e,PTL}}\right)^{0.5} \quad , \tag{2}$$

where $R_{\mathrm{eff,PTL}}$ is the effective tip radius at the contact depth and $h_{\mathrm{e,PTL}}$ is the elastic penetration depth under the force, $P_{\mathrm{PTL}}$, at which the PTL occurs.

It is difficult to produce diamond tips with ideal conospherical geometry; the effective tip radius usually varies with the penetration depth. The empirical relationship between effective tip radius and the penetration depth was determined, as described in Sec. II. A. The penetration depth relevant in this context is the contact depth, $h_{\mathrm{c,PTL}}$, which can be determined from $h_{\mathrm{e,PTL}}$:

$$h_{\mathrm{c,PTL}} = 0.5 h_{\mathrm{e,PTL}} \quad . \tag{3}$$

As mentioned, the onset of the PTL was studied using the partial unloading technique. Figure 2(a) shows an example of a partial unloading indentation sequence (change of force with time), as conducted in this study. Figure 2(b) displays the section of the force–displacement curve where the $P$–$h$ data of fully loaded and partially unloaded contact diverged and, thus, the PTL was assumed to start. For many indentation curves, the divergence of loading and unloading branch coincided with the pop-in event, whereas the divergence was detected before the occurrence of the pop-in in other cases.

#### 2. PTU

In case of PTU, the radius of the circle of contact, $a_{\mathrm{c,PTU}}$, can be calculated according to the method proposed by Field and Swain[23]:

$$a_{\mathrm{c,PTU}} = a_{\mathrm{c,max}} \left(h_{\mathrm{e,PTU}} / h_{\mathrm{e,max}}\right)^{0.5} \quad , \tag{4}$$

where $a_{\mathrm{c,max}}$ represents the radius of the contact circle at maximum force $P_{\mathrm{max}}$,

$$a_{\mathrm{c,max}} = \left(2 R_{\mathrm{eff,\ PTU}} h_{\mathrm{p,max}} - h_{\mathrm{p,max}}{}^{2}\right)^{0.5} \quad , \tag{5}$$

$h_{\mathrm{e,PTU}}$ is the elastic penetration depth at force $P_{\mathrm{PTU}}$,

$$h_{\mathrm{e,PTU}} = h_{\mathrm{t,PTU}} - h_{\mathrm{r,v}} \quad , \tag{6}$$

and $h_{\mathrm{e,max}}$ is the maximum elastic penetration depth

$$h_{\mathrm{e,max}} = h_{\mathrm{t,max}} - h_{\mathrm{r,v}} \quad , \tag{7}$$

where $h_{\mathrm{t,PTU}}$ is the total penetration depth at force $P_{\mathrm{PTU}}$, $h_{\mathrm{r,v}}$ is the virtual residual penetration depth after complete unloading, and $h_{\mathrm{t,max}}$ represents the total penetration depth at peak force $P_{\mathrm{max}}$. The virtual depth represents the maximum residual penetration that would be obtained without the interference of the described unloading events [see Fig. 2(c)].

The effective radius of the indenter tip, $R_{\mathrm{eff,\ PTU}}$, at the contact depth $h_{\mathrm{c,PTU}}$ can be determined from the previously described empirical relationship, whereas $h_{\mathrm{c,PTU}}$ can be obtained from

$$h_{\mathrm{c,PTU}} = \left(h_{\mathrm{t,PTU}} + h_{\mathrm{r,v}}\right)/2 \quad . \tag{8}$$

The maximum plastic penetration $h_{\mathrm{p,max}}$ after complete unloading is given by

$$h_{\mathrm{c,max}} = \left(h_{\mathrm{t,max}} + h_{\mathrm{r,v}}\right)/2 \quad , \tag{9}$$

and $h_{\mathrm{r,v}}$ can be obtained from the following ratio

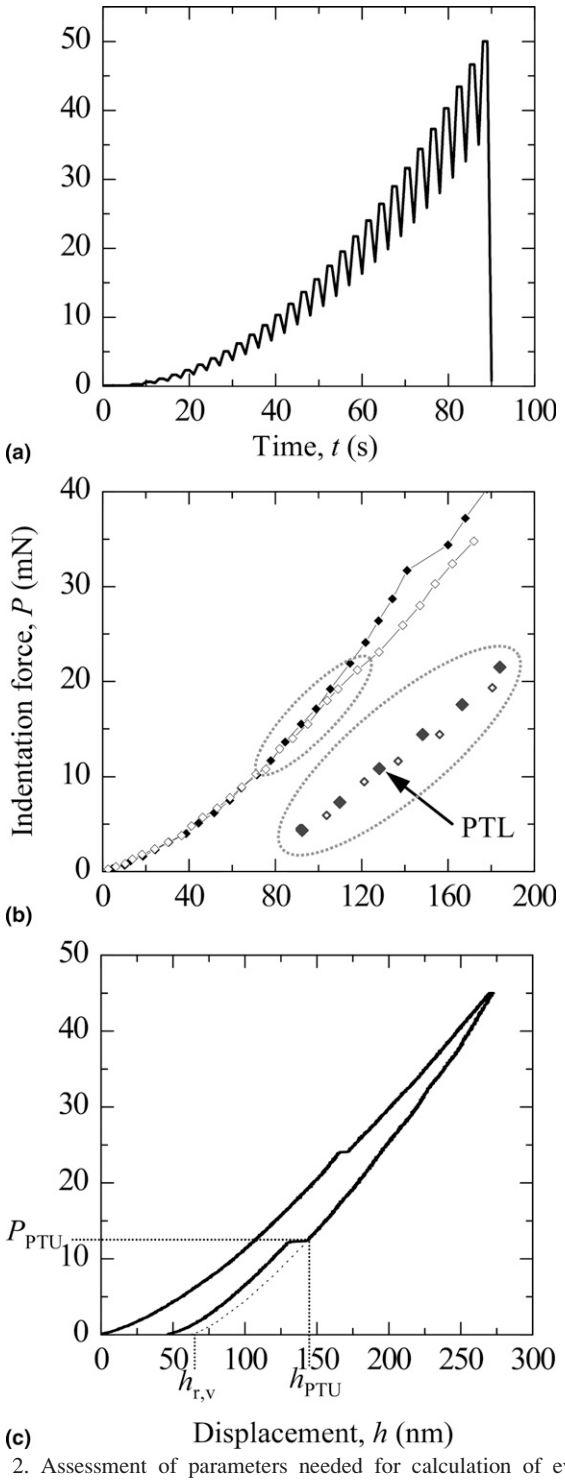


FIG. 2. Assessment of parameters needed for calculation of event pressures. In partial unloading tests, in which the force $P$ was varied with time $t$ as displayed in an example in (a). The presumed onset of PTL is indicated by the divergence between the force ($P$)-displacement ($h$) data of fully loaded (◇) and partially unloaded (◇) points in (b). Each (fully loaded, partially unloaded) point is the ($P$,$h$) pair corresponding to a force (peak, valley) in (a). The lines between the points were drawn to guide the eye. (c) Shows the determination from the indentation unloading curve of the virtual residual penetration depth $h_{r,v,}$ as well as the specific force ($P_{PTU}$) and penetration depth ($h_{PTU}$).

$$h_{r,v} = [h_{t,PTU}(P_{max}/P_{PTU})^{2/3} - h_{t,max}] / [(P_{max}/P_{PTU})^{2/3} - 1] \quad . \tag{10}$$

The data for determination of the parameters $P_{PTU}$ and $h_{t,PTU}$ essential to the calculations were taken from the force–displacement curves, as illustrated in Fig. 2(c).

## IV. RESULTS AND DISCUSSION

### A. Effect of crystallographic orientation on PTL

A dependence of the PTL pressure on crystallographic orientation in indentation tests was first reported by Gupta and Ruoff.[7] A clear difference in the PTL pressures for the various crystallographic orientations was also observed in the statistical evaluation here (Fig. 3). The $p_{PTL}$ value (given as mean ± standard deviation) decreases from 12.0 ± 0.8 GPa for Si(001) to 10.5 ± 0.6 GPa for Si(110), and 8.8 ± 0.9 GPa for Si(111), which is in good agreement with the data reported by Ruoff and Gupta and in other studies that were conducted mostly for the Si(001) orientation (Table I). This is the first time that a value for the PTL has been reported for Si(110) in indentation tests.

It has been proposed that a greater degree of superposed deviatoric loading increases the tendency for phase transformation under hydrostatic pressure.[2] The previous results for the measured $p_{PTL}$ variation with orientation are consistent with this idea if incipient slip on the primary slip system of fcc Si-I (slip planes {111}, slip directions ⟨110⟩) is considered a precursor to the primary phase transformation. Consideration of the

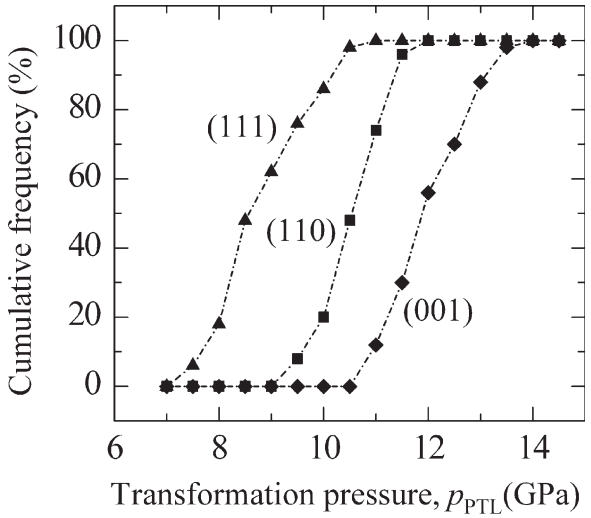


FIG. 3. Effect of the crystallographic orientation on the PTL pressure. The distribution of the values of the PTL pressure ($p_{PTL}$) is shown as cumulative percentage over defined pressure values for the orientations Si(001), Si(110), and Si(111).

TABLE I. Summary of frequency of occurrence, average, standard deviation, and observed pressure range of the event pressure of various loading (L) and unloading (UL) events for the tested Si orientations.

| Event | Orientation | Frequency | Average (GPa) | Standard deviation (GPa) | Pressure range[a] (GPa) | Pressure values reported in literature (GPa) |
|---|---|---|---|---|---|---|
| Pi | Si(100) | 50/50 | 12 | 0.8 | 10.7 to 13.3 (L) | 13.3,[28] 12,[7] 11.8 ± 0.6,[21] 9.9[37] |
| | Si(110) | 50/50 | 10.5 | 0.6 | 9.3 to 11.5 (L) | ... |
| | Si(111) | 50/50 | 8.8 | 0.9 | 7.4 to 10.4 (L) | 9.5 to 11,[22] 8,[7] |
| E | Si(100) | 18/450 | 8.0 | 0.2 | 6.0 to 4.6 (UL) | 5.5 to 4.5,[18] 4[38] |
| | Si(110) | 113/450 | 6.0 | 0.8 | 7.3 to 4.4 (UL) | ... |
| | Si(111) | 65/450 | 6.1 | 0.7 | 7.4 to 5.2 (UL) | 6.5 to 3.5[32] |
| P | Si(100) | 73/450 | 7.7 | 1.0 | 8.9 to 5.4 (UL) | 9.1 to 7.5,[21] 8.5 to 5,[18] 8.4[28] |
| | Si(110) | 99/450 | 8.5 | 1.0 | 10.2 to 7.0 (UL) | ... |
| | Si(111) | 187/450 | 8.3 | 1.1 | 10.6 to 6.6 (UL) | 11.0 to 4.5,[32] 9.5 to 3.5[22] |
| K | Si(100) | 154/450 | 7.7 | 0.9 | 9.0 to 6.2 (UL) | ... |
| | Si(110) | 166/450 | 9.6 | 1.2 | 11.4 to 7.4 (UL) | ... |
| | Si(111) | 173/450 | 9.1 | 1.6 | 11.4 to 6.6 (UL) | 12 to 8,[32] 10.5 to 3.5[22] |

Pop-in, (Pi); elbow (E, includes elbows and EP-elbows), kink pop-out (K) pop-out; pop-out (P, includes pop-outs and EP-pop-outs). Reference literature data are given for comparison.

[a]Covers the range from 5–95% of occurrence.

loading directions relative to the slip planes suggest resolved shear stresses on {111} planes for the $[00\bar{1}]$, $[0\bar{1}\bar{1}]$, and $[\bar{1}\bar{1}\bar{1}]$ loading directions in the ratios $1 : \sqrt{2} : \sqrt{3}$. The increased deviatoric loading for Si (110) and Si(111) orientations presumably facilitated plastic deformation processes leading to decreased transformation pressures. Information about the active slip systems for the different loading directions may be obtained from the residual stress maps collected by CRM. Certainly, the stress field changes in and around the indented region during loading and unloading, and the relevance of data from the residual stress field is limited regarding the interpretation of the dynamic slip processes giving rise to the stress changes and the ultimate residual field. However, the location of active slip systems should not change during loading and should be indicated by a residual stress feature caused by the plastic deformation. Figure 4 shows the spatial distribution of the residual stress field around indentations, produced at the same maximum force, determined by CRM. The residual field differs significantly among the three tested orientations. On the basis of the {111} slip planes available for a given loading direction, the stress field should exhibit either fourfold for Si(001), threefold for Si(111), or twofold symmetry for Si(110). This was in fact observed. These observations confirm the idea that the observed differences in onset pressure for the primary transformation in Si arise from local mechanistic effects associated with the ease of plastic deformation (transformation) on particular crystal planes.

## B. Effect of crystallographic orientation on PTU

### 1. Correlation of unloading events with PTU phases

Using CRM, it was found that Si-I was the only phase present in elastically deformed regions, as expected. At small indentation forces, some indentation curves displayed signs of plastic deformation and primary phase transformation (pop-in event), but no discontinuities of any kind were observed in the unloading segment. Furthermore, CRM of those indentations did not show any evidence for the formation of PTU, leading to the conclusion that the volume of material transformed in PTU at these forces is probably too small and possibly located too close to the surface to be detected by indentation or CRM. Bradby et al.[29] identified a thin zone of transformed material directly beneath the indenter in a TEM study of spherical indentations, although the unloading segment of the load–displacement curves did not display any PTU-related events.

For indentations exhibiting elbow events, *a*-Si was identified as the dominant phase in the residual impression. Almost identical compositions, mixtures of Si-II and Si-XII, were found for indentations exhibiting pop-out and kink pop-out events. In addition to those phases, *a*-Si was detected when an elbow preceded the pop-out event. The CRM results are consistent with previously reported observations that the occurrence of elbow event corresponds to the presence of *a*-Si and pop-out events are associated with the generation of crystalline high-pressure phases.[18,22,29,34]

### 2. Occurrence of unloading events as function of maximum load

The observed frequency of unloading events is presented in Fig. 5 for varying maximum forces applied to the differently oriented Si wafers.

Exclusively elastic behavior in all of the indentation tests was observed only for Si(100) and then only at the smallest maximum force applied in this study. However, elastic behavior was the predominant classification in

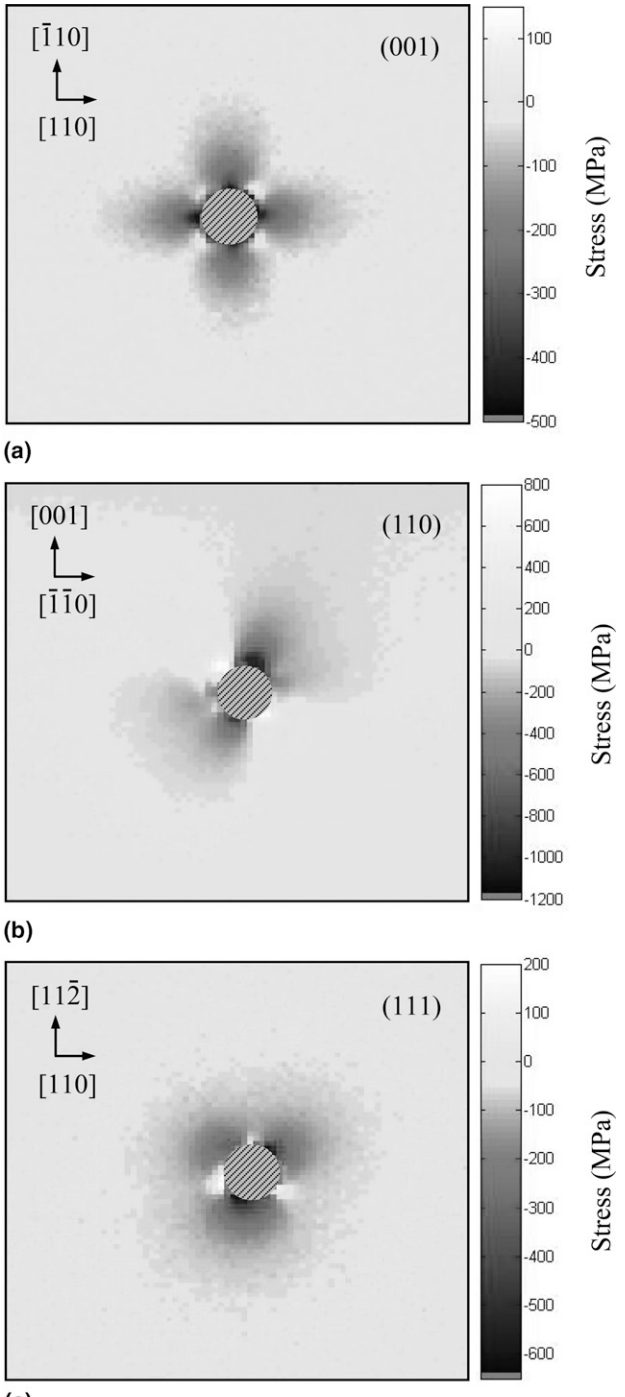


FIG. 4. Effect of crystallographic orientation on the residual stress. Representative stress patterns mapped by confocal Raman microscopy are shown for indentations produced at 80 mN maximum load on (a) Si(001)-oriented, (b) Si(110)-oriented, and (c) Si(111)-oriented surfaces. The scan size was set to 20 μm × 20 μm. The relevant crystallographic directions are indicated.

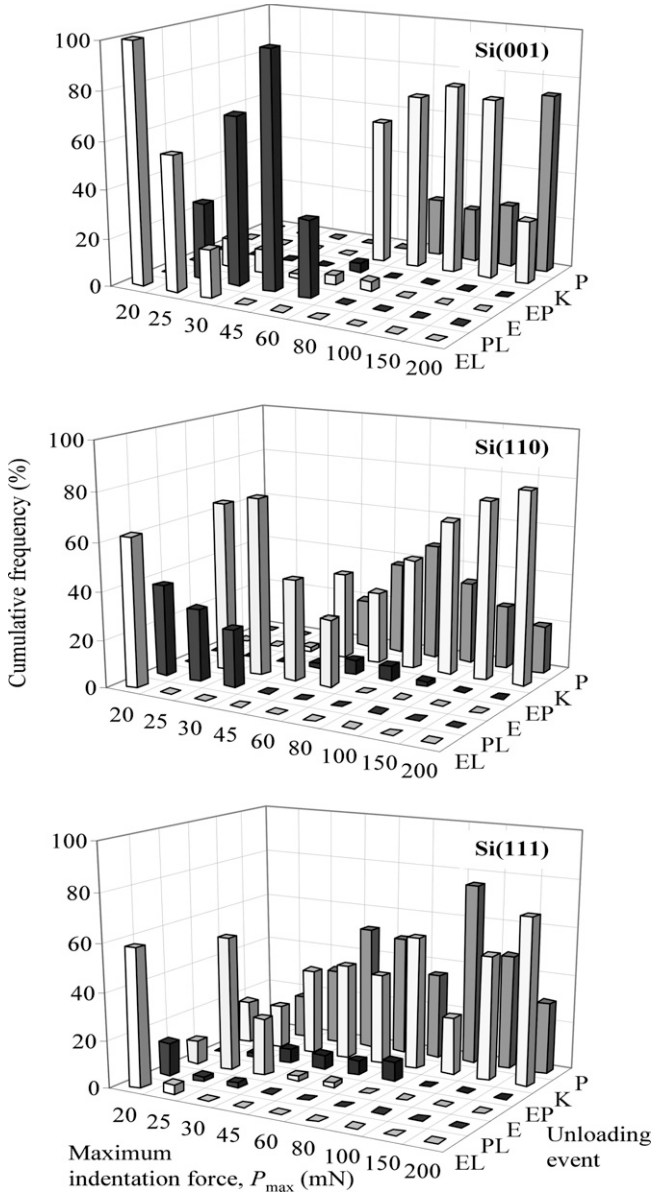


FIG. 5. Effect of the crystallographic orientation on the occurrence of unloading events. The occurrence in percentage of classified unloading events is shown for varying maximum forces $P_{max}$ applied on Si (001)-oriented, Si (110)-oriented, and Si(111)-oriented surfaces. Classified events: EL, elastic behavior; PL, plastic behavior; E, elbow; EP, elbow followed by pop-out; K, kink pop-out; and P, pop-out event.

tests at 25 mN for Si(001) as well as at 20 mN for the Si (110) and Si(111) orientations.

The frequency of indentations exhibiting plastic behavior (without showing a PTU-related event) increased from 0–98% when the maximum force was increased from 20 to 45 mN on Si(100), but dropped to significantly smaller frequency at 60 mN in favor of the greater occurrence of kink pop-out events. For the Si(110) orientation, significant portions of the indentation curves exhibited plastic behavior already at 20 mN as well as at 25 and 30 mN. Contrary to this, curves with plastic behavior were observed only occasionally in tests at maximum forces between 20 and 30 mN for Si(111).

Only a few elbow events were observed in tests at maximum forces ranging from 25 to 80 mN on Si(001),

whereas it was the predominant classification of indentation curves measured on Si(110) at 25 and 30 mN. At 45 and 60 mN, the frequency of elbow events decreased, but still remained at a high level. In case of Si(111), elbow events occurred in the force range from 20 to 60 mN, but represented the dominant or a significant portion only at 25 and 30 mN, respectively.

An elbow followed by a pop-out was a relatively rare event under the given test conditions. It was observed only at 60 mN for Si(001), in small numbers between 45 and 100 mN, or between 25 to 100 mN for Si(110) and Si(111), respectively.

When kink pop-outs and regular pop-outs were added together, they were the predominate unloading event in the indentation tests starting at $P_{max} \geq 60$ mN for Si (001), $P_{max} \geq 45$ mN for Si(110), and $P_{max} \geq 30$ mN for Si(111). For all orientations, kink pop-outs appeared at smaller forces than regular pop-out events. For Si (001), kink pop-out occurred with greater frequency than pop-outs, except for 200 mN. For Si(110), the portions of kink pop-out and regular pop-out events are similar between 45 and 80 mN, but the frequency of kink pop-out events was significantly greater than that of regular pop-outs at greater loads. No trend in this regard was observed in the tests on Si(111), but the frequency of kink pop-out events was greater than that of pop-out events for most of the maximum forces.

The data reveal that the onset of plastic deformation was shifted to smaller forces for Si(110) and Si(111) compared to Si(001), and the threshold load for plastic deformation was smallest for Si(111) among the tested orientations. At 20 mN, phase transformations associated with PTU events were already initiated in a significant portion of indentation tests on Si(111), whereas only signs of plastic deformation without any indications of PTU were found for Si(110) at the same force.

The difference in threshold force for plastic deformation for various orientations might be related to variations in their elasticity. A measure of elasticity is the indentation modulus; the greater the indentation modulus the lower is the capability of the materials to deform elastically. The indentation modulus was determined for the three orientations in separate indentation tests using the Oliver–Pharr method.[33] The tests were conducted with the same spherical indenter as used in this study at loads guaranteeing a purely elastic response of the materials. The indentation modulus (given as mean $\pm$ standard deviation for 20 indentation tests) increased from $125 \pm 3$ GPa for Si(001), to $162 \pm 6$ GPa for Si(110), to $179 \pm 5$ GPa for Si(111), indicating a greater propensity to plastic deformation for Si(110) and Si(111) compared to Si(001).

As a consequence of the greater forces required for plastic deformation, the PTU on Si(001) was also observed at forces greater than those for the two other orientations, and the threshold force appeared to be well defined, as opposed to the more gradual increases in PTU observations for Si(110) and Si(111). Based on the greater percentage of PTU-associated events at 20 and 25 mN, it seems that the threshold forces for initiating PTU is least for Si(111) among the three orientations.

The occurrence of specific unloading events depended on the applied maximum force for all three crystallographic orientations. At smaller forces, elbows formed the majority of PTU-related unloading events, whereas more events involving pop-outs appeared at greater forces. A similar tendency was reported for Si(001)[15,16] and Si(111)[31] orientations. It was suggested that the transforming volume is probably too small to allow the Si-II to Si-XII phase transformation (associated with pop-out events) at small forces and, thus, *a*-Si (associated with elbow events) is preferably formed.[2] In addition to these indentation observations, Zarudi et al.[35] suggested a stress dependence for crystal growth of high pressure phases, perhaps leading to more pronounced crystalline structures at the greater maximum forces.

Besides the force applied, the type of secondary phase transformation (hence, the shape of the unloading curve) depends also on the unloading rate.[15,22,27,32,34] Above a critical unloading rate, there is insufficient time for nucleation of the crystalline phases and, thus, *a*-Si is formed.[15] The study here indicates that the critical unloading rate is influenced by the crystallographic orientation. As the results show, the probability of observing *a*-Si (elbows) on Si(001) with an unloading rate of 5 mN $s^{-1}$ is relatively small. This is consistent with other studies, in which unloading rates between 11 to 1000 mN $s^{-1}$ were applied to obtain reliably *a*-Si.[29,36] However, elbows represent the dominating unloading event for Si(110) and Si(111) at certain forces, so the critical unloading rate seems to be smaller for these two orientations compared to Si(001).

### C. PTU pressure

The $p_{PTU}$ values for the observed unloading events (given as means and standard deviations) as a function of the maximum force applied on the orientations Si (001), Si(110), and Si(111) are shown in Fig. 6. Attention should be given to the fact that Fig. 6(a) displays the pressure values calculated for the regular elbow event and for elbows embedded in an EP event (referred to as EP-elbows in further text). Accordingly, Fig. 6(b) shows the pressure values for single pop-outs and pop-outs embedded in an EP event (referred to as EP-pop-outs in further text). Furthermore, the data presented in Figs. 6(d)–6(f) and Table I combined the pressure values of the EP events and the corresponding single events, as they do not differ significantly [see Figs. 6(a) and 6(b)].

For all classifications, the event pressure increased with the applied maximum force. For example, the PTU

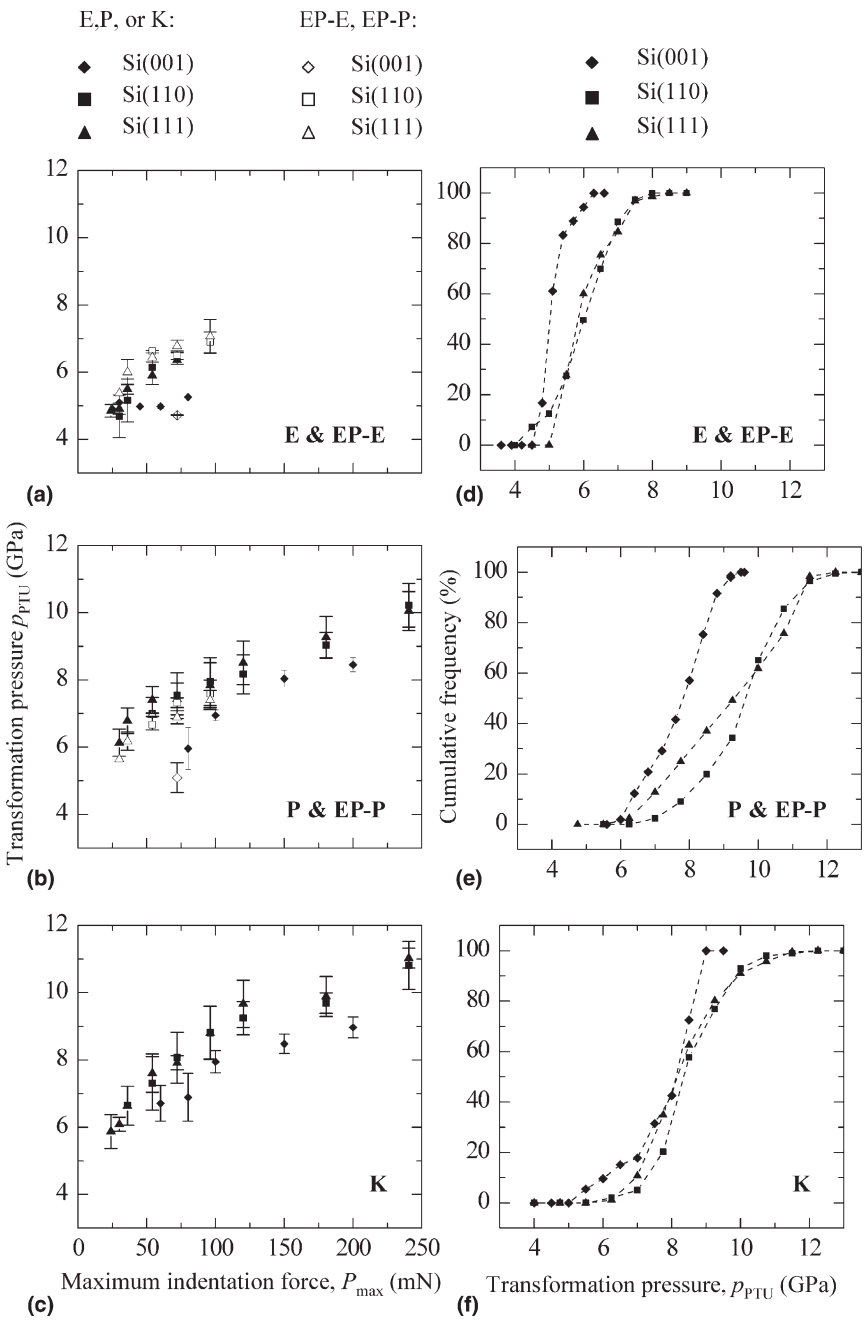


FIG. 6. Effect of the crystallographic orientation on the PTU pressure. The PTU pressure ($p_{PTU}$) as function of the maximum force applied is given for (a) elbows and EP-elbows, (b) single pop-out and EP-pop-outs, and (c) kink pop-outs events for the orientations Si(001), Si (110), and Si(111). The full symbols refer to single events, open symbols refer to EP-elbows and EP-pop-outs, respectively. The distribution of the $p_{PTU}$ values are shown as cumulative percentage for (d) elbows and EP-elbows, (e) pop-out and EP-pop-outs, and (f) kink pop-out events. The error bars represent the standard deviations of the measured values of the PTU pressure for a specific event calculated from all the tests, in which that event was observed.

pressure values for elbow events increased from 4.9 to 5.3 GPa for Si(001), 5.3 to 6.9 GPa for Si(110), and 5.5 to 6.9 GPa for Si(111) when the maximum force was increased from 25 to 30 mN for Si(001), 25 to 60 mN for Si(110), and 20 to 60 mN for Si(111). Because of the greater amount of constrained Si-II under the indenter at greater forces, the system is probably thermodynamically more unstable and the PTU starts sooner on unloading.[22] This trend was observed for all three Si orientations. For kink pop-out and pop-out events, such an effect was reported by Juliano et al.[22] in tests on Si(111). However, in their study, using a spherical indenter with much larger radius (13.5 μm), elbow events were not observed during unloading, although *a*-Si mixed with other crystalline phases was detected in the residual indentation. Except for the elbow events, the

rate the pressure changed with increasing maximum force was similar for the three orientations.

When comparing the actual $p_{PTU}$ values, it can be seen that the pressures for a specific unloading event are similar for Si(110) and Si(111), but significantly greater (between 13% and 38%) than those for Si(001). This holds true for all event classifications in this study. Furthermore, the pressure range associated with a given unloading event is larger for Si(110) and Si(111) than for Si(001) [Figs. 6(c)–6(f) and Table I]. The onset of the PTU at greater pressures for Si(110) and Si(111) compared to Si(001) might be explained in the following way. In case of Si (110) and Si(111) orientations, the plastic deformation, and combined with it the Si-I to Si-II phase transformation, starts at an earlier stage during loading than for Si (001) (see Sec. IV. A). Under the same maximum force, it can then be assumed that the volume of the Si-II phase is larger for those two orientations than for Si(100). Molecular dynamics (MD) simulations indeed have shown more significant internal slip and spreading of the phase transformation when loading perpendicular to an Si(110) surface compared to loading perpendicular to the Si(001) surface.[39] Another MD study revealed a more confined region of phase transformation under the indenter for Si (111) compared to the Si(001) orientation.[40] As mentioned earlier, the greater thermodynamic instability of a large constrained volume of material probably enabled the initiation of phase transformations at greater pressures.

The $p_{PTU}$ pressure values were greatest for kink pop-out events, followed by pop-out events and then elbow events. It is interesting to note that the ranking is in agreement with data obtained for Si(111) probed with a sharper (Berkovich) indenter,[32] but contradicts the results from tests performed with a blunter indenter (sphere with 13.5 μm radius), in which no significant difference was found in the pressure between both of those events.[22] Presumably, the variation in shear stress (smaller for the larger spherical indenter) is the cause for the discrepancy in results. The shear stress is an essential parameter for the initiation of phase transformation processes.[41]

## V. CONCLUSIONS

There are significant differences in the indentation deformation behavior of Si as a function of orientation. Si(001), Si(110), and Si(111) exhibit considerable differences in the events observed in force–displacement curves on spherical indentation in terms of the forces at which events occur, the frequency of occurrence of events at a given indentation force, and the way in which the occurrence frequency changes as a function of indentation force. The events (marked by changes in the derivative of the force–displacement curve) can be interpreted in terms of phase changes in Si induced by indentation and suggest a variation in the pressure required for the primary phase change (from semiconducting, Si-I, to metallic, Si-II) on loading as a function of orientation. Plastic deformation and the Si-I to Si-II phase transformation are initiated at smaller pressures during loading for Si(001), Si(110), and Si(111), respectively, consistent with an increasing deviatoric stress component increasing the tendency to transform. [Values for transformation pressures on Si(110) determined in indentation tests are reported for the first time.] The secondary phase transformations (to Si-III, Si-XII, and *a*-Si) on unloading also exhibit variations in pressure, compared to Si(100), the secondary phase transformations during unloading occur at greater pressures for Si(110) and Si(111). The critical unloading rate for amorphization during unloading appears to be dependent on indentation orientation, with that for Si(110) and Si(111) less than that of Si(001). Statistical analysis of the overall loading and unloading data suggests that the indentation behavior of Si(001) is different from that of Si(110) and Si(111), which are quite similar by comparison. Two important, related, technological implications follow from these observations. First, orientation dependence (anisotropy) in the contact behavior—both during and after contact—of Si should be taken into account when designing, fabricating, and operating Si devices that experience small-scale contacts or large stresses on different crystallographic planes. Second, parameters describing the contact behavior of Si determined using the Si(001) orientation, pervasive in the semiconductor microelectronics industry, may not be applicable to devices in which other orientations encounter contacts, such as the Si(110) sidewalls in MEMS devices and the Si(111) surfaces in photovoltaic devices. Further indentation experiments, including those at various unloading rates, should be performed to extend the observations here to devicelike conditions. In addition, TEM investigations of indented regions and simulations are required to gain more insight into the effects of the loading direction on the pressure and stress state and the structural changes during phase transformation processes.

## ACKNOWLEDGMENT

Any mention of commercial products in this article is for information only. It does not imply recommendation or endorsement by NIST.

## REFERENCES

1. A. Mujica, A. Rubio, and R.J. Needs: High-pressure phases of group-IV, III-V, and I-VI compounds. *Rev. Mod. Phys.* **75,** 863 (2003).
2. V. Domnich and Y. Gogotsi: Phase transformation in silicon under contact loading. *Adv. Mater. Sci.* **3,** 1 (2002).
3. O. Shimomura, S. Minomura, N. Sakai, K. Asaumi, K. Tamura, J. Fukushima, and H. Endo: Pressure-induced semiconductor-metal transitions in amorphous Si and Ge. *Philos. Mag.* **29,** 547 (1974).

4. J. Patten, H. Cherukuri, and J. Yan: Ductile regime machining of semiconductors and ceramics, in *High Pressure Surface Science and Engineering*, edited by Y. Gogotsi and V. Domnich (IoP, Institute of Physics, Bristol, 2004), p. 542.
5. A. Kovalchenko, Y. Gogotsi, V. Domnich, and A. Erdemir: Phase transformations in silicon under dry and lubricated sliding. *Tribol. Trans.* **45,** 372 (2002).
6. R. Rao, J.E. Bradby, and J.S. Williams: Patterning of silicon by indentation and chemical etching. *Appl. Phys. Lett.* **91,** 123113 (2007).
7. M.C. Gupta and A.L. Ruoff: Static compression of silicon in the [100] and in the [111] directions. *J. Appl. Phys.* **51,** 1072 (1980).
8. D.K. Sadana, S.W. Bedell, A. Reznicek, J.P. De Souza, K.E. Fogel, and H.J. Hovel: Strain engineering for silicon CMOS technology, in *ULSI Process Integration IV, Proceedings of the International Symposium* (Electrochemical Society, 2005), pp. 360–382.
9. L. Chengkuo: Novel H-beam electrothermal actuators with capability of generating bi-directional static displacement. *Microsyst. Technol.* **12,** 717 (2006).
10. A. Jain and H. Xie: An electrothermal SCS micromirror for large bi-directional 2-D scanning, in *13th International Conference on Solid-State Sensors and Actuators and Microsystems*, Digest of Technical Papers, 2005, pp. 988–991.
11. D. Moore, A. Wilson, and R. Ross: Simulated hail impact testing of photovoltaic panels, in *Proceedings, Annual Technical Meeting* (Institute of Environmental Sciences, 1978), pp. 419–430.
12. V.A. Letin, A.B. Nadiradze, and L.S. Novikov: Forecasting the influence of solid microparticles on space craft solar array, European Space Agency (special publication), ESA SP, n 589, in *Proceedings of the Seventh European Space Power Conference* (2005), pp. 453–458.
13. B.P. O'Connor, E.R. Marsh, and J.A. Couey: On the effect of crystallographic orientation on ductile material removal in silicon. *Precis. Eng.* **29,** 124 (2005).
14. H.T. Young, H-Y. Huang, and Y-J. Yang: A fundamental modeling approach for nano-grinding of silicon wafers, Materials Science Forum, Vol. 505–507, PART 1, Progress on Advanced Manufacture for Micro/Nano Technology 2005, in *Proceedings of the 2005 International Conference on Advanced Manufacture* (2006), pp. 253–258.
15. J. Jang, M.J. Lance, S. Wen, T.Y. Tsui, and G.M. Pharr: Indentation-induced phase transformations in silicon: Influences of load, rate and indenter angle on the transformation behavior. *Acta Mater.* **53,** 1759 (2005).
16. D. Ge, V. Domnich, and Y. Gogotsi: High-resolution transmission-electron-microscopy study of metastable silicon phases produced by nanoindentation. *J. Appl. Phys.* **93,** 2418 (2003).
17. S.V. Hainsworth, A.J. Whitehead, and T.F. Page: The nanoindentation response of silicon and related structurally similar materials, in *Plastic Deformation of Ceramics*, edited by R.C. Bradt, C.A. Brookes, and J.L. Routbort (Proc. of International Engineering Foundation Conference on the Plastic Deformation of Ceramics, Snowbird, UT, 1994), p. 173.
18. V. Domnich, Y. Gogotsi, and S. Dub: Effect of phase transformations on the shape of the unloading curve in the nanoindentation of silicon. *Appl. Phys. Lett.* **76,** 2214 (2000).
19. R.G. Jasinevicius, J.G. Duduch, and P.S. Pizani: The influence of crystallographic orientation on the generation of multiple structural phases generation in silicon by cyclic microindentation. *Mater. Lett.* **62,** 812 (2008).
20. R.F. Cook: Strength and sharp contact fracture of silicon. *J. Mater. Sci.* **41,** 841 (2006).
21. E.R. Weppelmann, J.S. Field, and M.V. Swain: Observation, analysis, and simulation of the hysteresis of silicon using ultra-micro-indentation with spherical indenters. *J. Mater. Res.* **8,** 830 (1993).
22. T. Juliano, V. Domnich, and Y. Gogotsi: Examining pressure-induced phase transformations in silicon by spherical indentation al study. *J. Mater. Res.* **19,** 2099 (2004).
23. J.S. Field and M.V. Swain: A simple predictive model for spherical indentation. *J. Mater. Res.* **8,** 297 (1993).
24. R. Sherman: Carbon dioxide snow cleaning. *Part. Sci. Technol.* **25,** 37 (2007).
25. C.E. Jordan, S.J. Stranick, R.R. Cavanagh, L.J. Richter, and D.B. Chase: Near-field scanning optical microscopy incorporating Raman scattering for vibrational mode contrast. *Surf. Sci.* **433–435,** 48 (1999).
26. V.T. Srikar, A.K. Swan, M. Selim Ünlü, B.B. Goldberg, and S.M. Spearing: Micro-Raman measurement of bending stresses in micromachined silicon flexures. *J. Microelectromech. Syst.* **12,** 779 (2003).
27. A. Kailer, K.G. Nickel, and Y.G. Gogotsi: Raman microspectroscopy of nanocrystalline and amorphous phases in hardness indentations. *J. Raman Spectrosc.* **30,** 939 (1999).
28. J.S. Williams, Y. Chen, J. Wong-Leung, A. Kerr, and M.V. Swain: Ultra-micro-indentation of silicon and compound semiconductors with spherical indenters. *J. Mater. Res.* **14,** 2338 (1999).
29. J.E. Bradby, J.S. Williams, J. Wong-Leung, M.V. Swain, and P. Munroe: Mechanical transformation in silicon by micro-indentation. *J. Mater. Res.* **16,** 1500 (2001).
30. H. Saka, A. Shimatani, M. Suganuma, and M. Suprijadi: Transmission electron microscopy of amorphization and phase transformation beneath indents in Si. *Philos. Mag. A* **82,** 1971 (2002).
31. D. Ge, A.M. Minor, E.A. Stach, and J.W. Morris, Jr.: Size effects in the nanoindentation of silicon at ambient temperature. *Philos. Mag.* **86,** 4069 (2006).
32. T. Juliano, Y. Gogotsi, and V. Domnich: Effect of indentation unloading conditions on phase transformation induced events in silicon. *J. Mater. Res.* **18,** 1192 (2003).
33. W.C. Oliver and G.M. Pharr: An improved technique for determining hardness and elastic modulus using load and displacement sensing indentation experiments. *J. Mater. Res.* **7,** 1564 (1992).
34. A. Kailer, Y.G. Gogotsi, and K.G. Nickel: Phase transformations of silicon caused by contact loading. *J. Appl. Phys.* **81,** 3057 (1997).
35. I. Zarudi, L.C. Zhang, and J. Zou: The R8-BC8 phases and crystal growth in monocrystalline silicon under microindentation with a spherical indenter. *J. Mater. Res.* **19,** 332 (2004).
36. S. Ruffell, J.E. Bradby, and J.S. Williams: High pressure crystalline phase formation during nanoindentation: Amorphous versus crystalline silicon. *Appl. Phys. Lett.* **89,** 091919 (2006).
37. J.E. Bradby, J.S. Williams, J. Wong-Leung, and M.V. Swain: Transmission electron microscopy observation of deformation microstructure under spherical indentation in silicon. *Appl. Phys. Lett.* **77,** 3749 (2000).
38. V. Domnich, Y. Gogotsi, and M. Trenary: Identification of pressure-induced transformations using nanoindentation, in *Fundamentals of Nanoindentation and Nanotribology II*, edited by S.P. Baker, R.F. Cook, S.G. Corcoran, and N.R. Moody (Mater. Res. Soc. Symp. Proc. **649,** Warrendale, PA, 2001), Q8.9.1.
39. Y-H. Lin, T-C. Chen, P-F. Yang, S-R. Jian, and Y-S. Lai: Atomic-level simulations of nanoindentation-induced phase transformation in mono-crystalline silicon. *Appl. Surf. Sci.* **254,** 1415 (2007).
40. D.E. Kim and S.I. Oh: Atomistic simulation of structural phase transformations in monocrystalline silicon induced by nanoindentation. *Nanotechnology* **17,** 2259 (2006).
41. T. Vodenitcharova and L.C. Zhang: A mechanics prediction of the behaviour of mono-crystalline silicon under nano-indentation. *Int. J. Solids Struct.* **40,** 2989 (2003).